Metallomics

Accepted Manuscript

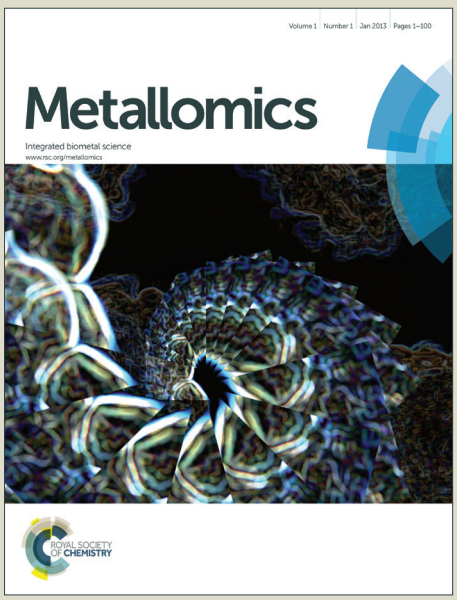

ROYAL SOCIETY OF CHEMISTRY

www.rsc.org/metallomics

Metallomics

Dynamic Article Links ►

Cite this: DOI: 10.1039/c0xx00000x

www.rsc.org/xxxxxx

Paper

Aberrant zinc binding to immature conformers of metal-free copper-zinc superoxide dismutase triggers amorphous aggregation

Sónia S. Leal[a,‡], Joana S. Cristóvão[a,‡], Antje Biesemeier[b], Isabel Cardoso[c], Cláudio M. Gomes[a]

Received (in XXX, XXX) Xth XXXXXXXXX 20XX, Accepted Xth XXXXXXXXX 20XX

DOI: 10.1039/b000000x

Superoxide dismutase 1 (SOD1) is a Cu/Zn metalloenzyme that aggregates in amyotrophic lateral sclerosis (ALS), a fatal neurodegenerative disorder. Correct metal insertion during SOD1 biosynthesis is critical to prevent misfolding; however Zn^{2+} can bind to the copper-site leading to an aberrantly metallated protein. These effects of Zn^{2+} misligation on SOD1 aggregation remain to be explored, even though Zn^{2+} levels are upregulated in ALS motor neurons. Here we use complementary biophysical methods to investigate Zn^{2+} binding and its effects on the aggregation of three immature metal-free SOD1 conformers that represent biogenesis intermediates: dimeric, monomeric and reduced monomeric SOD1. Using isothermal titration calorimetry we determined that Zn^{2+} binds to all conformers both at the zinc- as well as to the copper-site; however Zn^{2+} binding mechanisms to the zinc-site have distinct characteristics across immature conformers. We show that this 'zinc overload' of immature SOD1 promotes intermolecular interactions, as evidenced by dynamic light scattering and ThT fluorescence kinetic studies. Analysis of aged zinc-induced aggregates by energy-dispersive X-ray and electron energy-loss spectroscopy shows that aggregates integrate some Zn^{2+}. In addition, electron diffraction analysis identifies nano-scaled crystalline materials and amyloid fibril-like reflections. Transmission electron microscopy reveals that Zn^{2+} diverts the SOD1 aggregation pathway from fibrils to amorphous aggregate, and electrophoretic analysis evidences an increase in insoluble materials. Overall, we provide evidence that aberrant zinc coordination to immature conformers broadens the population of SOD1 misfolded species at early aggregation stages and provide evidence for a high structural polymorphism and heterogeneity of SOD1 aggregates.

Introduction

Superoxide dismutase 1 (SOD1) is a Cu/Zn metalloenzyme[1] implicated in the formation of proteinaceous toxic aggregates in the affected motor neurons of familial and sporadic forms of amyotrophic lateral sclerosis (ALS)[2]. SOD1 is a very stable homodimeric metalloenzyme when fully assembled, but is rather unstable and aggregation prone in the metal-free apoprotein form. Each SOD1 subunit binds one Cu^{2+} and Zn^{2+} in a binuclear site. SOD1 is a β-protein comprising a β-barrel flanked by two major loops, the 'electrostatic' and 'zinc' loops that together shape the active site pocket. Cu^{2+} is directly coordinated to residues within the two loops while Zn^{2+} binds to the residues in zinc loop which is linked to the β-barrel by an intra-subunit disulfide bridge[3]. In the absence of coordinated Cu^{2+} and Zn^{2+} the β-barrel and the dimer interface remain intact but the loops evidence increased disorder[4]. These post-translation modifications significantly affect SOD1 stability and propensity to aggregate which is a well-known feature in ALS pathology. Point mutations in SOD1 can aggravate this situation but since familial ALS are a minority of cases, other mechanisms affecting normal SOD1 must underlie the development of pathological aggregates[5].

Mounting evidence suggests that immature conformers are likely the key precursors of SOD1 aggregation events [6], whereas native metallation, and in particular correct Zn^{2+} coordination plays a central role in the regulation of SOD1 propensity to aggregate[7]. Intracellular SOD1 maturation is suggested to proceed with the initial coordination of Zn^{2+} to the reduced monomer which organizes the SOD1 connecting loops and allows the insertion of Cu^{2+} via the CCS machinery and disulfide bond formation with concomitant dimerization[5a, 8]. However, it was shown that exposure of apo SOD1 immature conformers to labile Zn^{2+}, *in vitro* at physiological pH, generates a SOD1 conformer where Zn^{2+} is bound to the native zinc site but is also aberrantly bound to the Cu site, forming a di-zinc protein (Zn,Zn-SOD1)[9]. In contrast, an *in cell* NMR study showed that within the cytoplasm environment, immature SOD1 selectivity coordinates zinc exclusively to the zinc site[10]. In spite of this accurate insertion of zinc, no metallo-chaperone protein that loads zinc into apo SOD1 has yet been found. It is thus possible that neurologic or traumatic injury conditions resulting in Zn^{2+} upregulation [11] compromise the selectivity of SOD1 metallation. In fact, zinc dyshomeostasis has emerged as an important player of pathological processes in disease[12], including ALS[13] and other neurodegenerative diseases[14]. Labile zinc levels are significantly elevated in the brain and spinal cord of SOD1 transgenic ALS mice models[15], where zinc is found to co-accumulate with SOD1 clinical mutants[16] and to accelerate motor neuron death[17]. However, a possible role for this labile Zn^{2+} pool in SOD1 misfolding through aberrant coordination remains to be investigated. In order

to better understand the mechanisms and possible consequences of abnormal metallation we carried out a biophysical analysis of Zn^{2+} binding to different immature metal-free SOD1 conformers, as experimental models of species that are populated during SOD1 biogenesis. Those conformers are plausible targets for aberrant Zn^{2+} coordination and are therefore good models to establish a mechanistic framework to test binding and effects on SOD1 aggregation.

Results and Discussion

Isothermal titration calorimetry analysis of Zn^{2+} binding to metal-free immature SOD1 conformers

In order to characterize Zn^{2+} binding to apo SOD1 at different stages of its maturation process, we have used isothermal titration calorimetry (ITC) and three models: oxidized SOD1 dimer ($dSOD1^{S-S}$), oxidized SOD1 monomer ($mSOD1^{S-S}$) and reduced SOD1 monomer ($mSOD1^{SH}$). The monomeric forms are engineered variants in which interacting residues at the dimer interface have been modified to prevent dimer assembly, resulting in a SOD1 monomer with preserved fold but increased dynamics[18]. This study was done at pH 7.4 and at 37°C to mimic conditions of the cell physiology.

$dSOD1^{S-S}$

The isothermogram of Zn^{2+} binding to $dSOD1^{S-S}$ clearly shows at least two overlapped binding processes **(Fig. 1A)**. The first transition saturating at a molar ratio of ≈ 2 corresponds to Zn^{2+} binding to each of the two zinc-sites in the homodimer, as it was shown that at this stoichiometry Zn^{2+} binds preferentially to the zinc-site[7d, 19]; the second transition saturating at a molar ratio of ≈ 4 indicates binding to two additional sites. We further titrated the zinc-saturated sample with Cu^{2+} at up to a molar ratio of Cu^{2+}/SOD1 of 15 and did not observe additional binding transitions (data not shown), suggesting that those sites were occupied and that aberrant coordination of Zn^{2+} to the copper-site prevents subsequent Cu^{2+} binding. This conclusion is in agreement with a previous study on the metal-reconstitution of apo SOD1 which showed that if an excess of labile Zn^{2+} is initially added to apoprotein at neutral pH (as we have done here), this deflected Cu^{2+} from binding to its native site[20].

Our results could not however be described by any of the simple interaction models of two sets of sites or sequential sites. Instead, we employed a more complex model comprising multiple binding sites as described in[21]. Although this fitting algorithm can model systems with up to four overlapping binding processes, the best fit to the $dSOD1^{S-S}$ Zn^{2+} binding data corresponds to a model of three sites **(Fig. 1A)**. The computed parameters suggest that Zn^{2+} binds to the two zinc-sites (Zn1 and Zn2) via dissimilar mechanisms and affinities, while Zn^{2+} binding to the two copper-sites in the homodimer (Cu1 and Cu2) occurs through a parallel mechanism with undistinguishable energetics **(Table 1)**. All binding events are enthalpically driven through favourable intermolecular interactions.

It is noteworthy the large gap in affinity between the two Zinc-sites in the homodimer. Indeed, binding of Zn^{2+} to the SOD1 zinc-sites is intrinsically complex as evidenced by the previously described negative cooperativity effects[7b], although the two zinc-sites are structurally identical in the homodimer. Indeed, binding of the first Zn^{2+} per apoprotein homodimer was reported to have a more profound effect on the protein structure than binding of the second Zn^{2+} [7b]. We also find evidence in support of the previously proposed "subunit swapping" mechanism[7b]. The fact that we calculate asymmetrical binding stoichiometries for binding of Zn^{2+} to the two zinc-binding sites (n=1.39±0.02 and n2=0.21±0.04) can likely be inputted to that mechanism according to which initial binding of one Zn^{2+} to the apo homodimer produces a one-zinc dimer which can then exchange subunits with a second equivalent one-zinc dimer, resulting in a two-zinc homodimer and one apo homodimer[7b]. The consequence of this postulate is that a higher number of Zn^{2+} participate in the binding to the first high affinity Zn binding site. In agreement, when ITC titrations were performed at lower SOD1 concentrations, we observed a decrease in the stoichiometry of the Zn1 site and an increase in that of Zn2 site (Fig S1, Table S1).

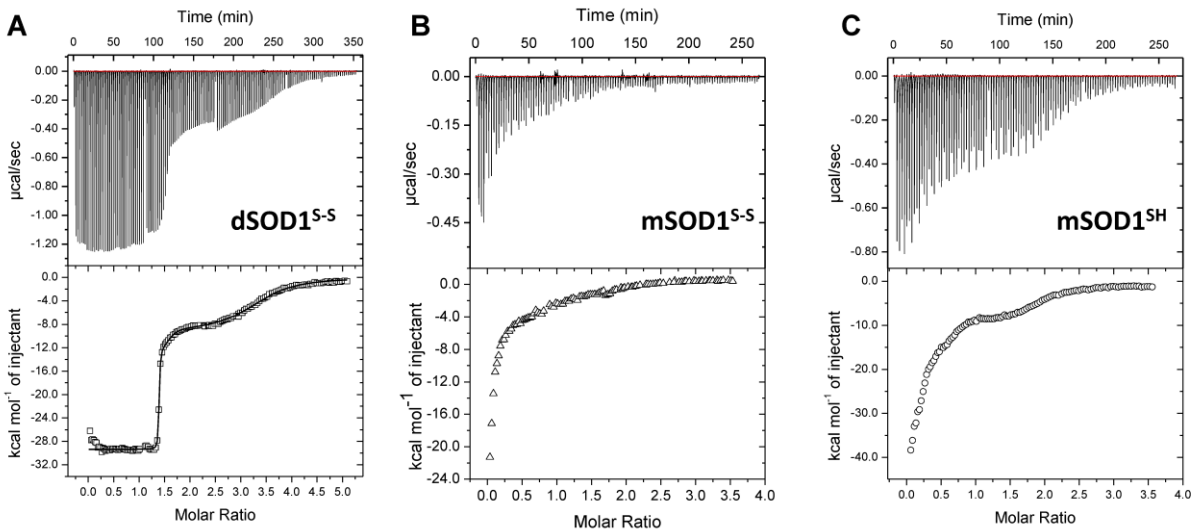

Figure 1 - Isotermal titration calorimetry analysis of Zn^{2+} binding to metal free immature SOD1 conformers. $dSOD1^{S-S}$ (A), $mSOD1^{S-S}$ (B) and $mSOD1^{SH}$ (C) at 37ºC and pH 7.4. The upper panel shows the raw heats of binding and the lower panel shows the integrated data obtained after subtracting the heat of dilution from the. Representative of n=3 experiments. See also Table 1.

Metallomics

Dynamic Article Links ►

Cite this: DOI: 10.1039/c0xx00000x

www.rsc.org/xxxxxx

Paper

Table 1: Estimated parameters of Zn binding to dSOD1^{S-S} [a]

	n	K_a (M^{-1})	ΔH (Kcal/mol^{-1})	ΔG (Kcal/mol^{-1})	ΔS (cal/mol^{-1}/deg)
I	1.39 ±0.02	2.1 x10^{10}	-29.3 ± 0.1	-14.6	-14.64
II	0.21 ±0.04	8.2 x10^{6}	-13.0 ± 1.5	-9.8	-3.13
III	1.94 ±0.06	1.7 x10^{5}	-9.1 ± 0.3	-7.43	-1.65

[a] Zn^{2+} binding to 80μM of dSOD1^{S-S} in 50 mM TRIS pH 7.4 and 37ºC. Apo SOD1 dimer contains 2 zinc-sites and 2 copper-sites, one per monomer. The roman numbering in the table refers to binding events associated with one Zn^{2+} binding to the first zinc-site Zn1 (I), to one Zn^{2+} binding to the second zinc-site in the apo dimer, Zn2 (II), and to binding of two Zn^{2+} to the two copper-sites (Cu1 and Cu2) in the apo dimer.

mSOD1^{S-S}

In contrast to the previous case, the isothermogram of Zn^{2+} binding to mSOD1^{S-S} denotes a lack of a plateau for the initial major enthalpy favorable transition, as well as for the poor-outlined second binding process, disclosing low enthalpic variation **(Fig. 1B)**. Although no model could accurately describe the measured heat exchange, the hyperbolic isotherms may indicate that the mSOD1^{S-S} conformer binds labile Zn^{2+} with low affinity. However, the low stoichiometry of Zn^{2+} binding (n<1) associated with this strong and favorable binding process, suggests that the mSOD1^{S-S} conformers are not equally competent for Zn^{2+} binding, in agreement with recently NMR findings[22]. Therefore, we can only speculate that the Zn^{2+} binding affinity to the mSOD1^{S-S} conformer is likely distinct from that of binding to the dimer. The differences in Zn^{2+} binding may result from the fact that monomeric SOD1 has a high conformational flexibility and is known to populate a broad and dynamic range of conformers[4b]. Adding complexity to this already rather heterogenous system, it was also suggested that in the mSOD1^{S-S} conformation, Zn^{2+} ion can exchange between the zinc- and the copper- sites[7a].

mSOD1^{SH}

The investigation of Zn^{2+} binding to the reduced monomeric SOD1 conformer is particularly significant as this process has been suggested to occur in this earliest state of folding *in vivo* [8, 23]. The isothermogram of Zn^{2+} binding to mSOD1^{SH} reveals two binding processes: a primarily process featuring a high enthalpic variation that saturates at a molar ratio of ≈ 1 and a second binding process that saturates at a molar ratio above 2 **(Fig. 1C)**. Again, no model could be accurately used in data fitting but it is reasonable to suggest that the binding process associated with the prominent enthalpic variation corresponds to the interaction with the relatively solvent-exposed zinc site in the SOD1 monomer conformer that thus strongly binds Zn^{2+} and greatly impacts on SOD1 overall structure, in contrast with the Cu site that is yet disorganized[4b, 7c, 24]. Although reduction of the SOD1 native disulfide bridge that links the zinc-loop to the β-sheet barrel does not significantly change the structural features of the monomer, it further disorders the zinc-loop, increasing its conformational flexibility[25]. This factor adds to the heterogeneity of the system but ultimately Zn^{2+} binding to the zinc-site organizes the copper-site ligands to allow misligation of Zn^{2+}, which we presume to correspond to the second binding event **(Fig. 1C)**. Nevertheless, the possibility that this results from binding to other heterogeneous zinc-sites in less populated SOD1 monomers cannot be totally excluded, also for mSOD1^{S-S}.

Labile Zn^{2+} induces aggregation of SOD1 conformers

We then analysed the effect of Zn^{2+} binding to apo SOD1 conformers upon 1h of incubation at 37 ºC, at distinct Zn^{2+}/SOD1 ratios, to investigate possible effects on protein aggregation. We used dynamic light scattering (DLS), a highly sensitive technique that allows to determine minute variations in the hydrodynamic properties and protein oligomerization.

dSOD1^{S-S}

The DLS size distribution profile of the apoprotein dSOD1^{S-S} was found to be monomodal by volume with a mean peak averaging at an hydrodynamic diameter of 5.30±0.07 nm **(Fig. 2A)**, which agrees well with the diameter of the SOD1 dimer[26].

Upon binding of Zn^{2+}, a slight decrease trend is observed at up to a molar ratio of 3 suggesting some structural compaction. This likely result from progressive ordering and constraining of the zinc-loop regions upon Zn^{2+} binding to the zinc-site, which would be otherwise disordered[4b].

At molar ratios above 3, the mean hydrodynamic diameter increases up to 6.8 nm as well as the mean light scattering intensity (Kcps), a DLS parameter that evaluates the scattering intensity variation and increases with the presence of larger particles **(Fig. 2A, inset)**. This suggests the formation of SOD1 oligomers which however do not yield a multimodal distribution at higher molar ratios **(Fig. 2A)**. This is actually what would be expected if the population of these oligomers is very low[27] relatively to that of dimeric zinc-containing SOD1. We have further investigated this by computing the Z-average size, a hydrodynamic parameter which is very sensitive to minute populations of large oligomeric species. This analysis corroborates the existence of a minute population of oligomers, as a drastic increase is the z-average size to above 200 nm is observed **(Supplementary Fig. S2)**. Interestingly, the larger population of dSOD1^{S-S} becomes more homogeneous upon full zinc metallation as evidenced from the decrease in the mid-height of the size distribution peaks, which narrow from 1.1 to 0.4 nm at increasing molar ratios **(Fig. 2A)**. This is in agreement with the fact that metal-free dSOD1^{S-S} is known to sample a large range of conformations[28], which decrease upon metal-binding.

We have then tested if Cu^{2+} binding to dSOD1^{S-S} would have similar effects to those of Zn^{2+}. In control DLS experiments at up to a molar ratio of Cu^{2+}/SOD1 of 4 we have not observed changes nor oligomerization (data not shown). Interestingly, analysis of structures of aggregation-prone ALS variants SOD1 D124V and SOD1 H80R which have disrupted zinc-sites shows that Zn^{2+}

rather than Cu^{2+} occupies the copper-site[29]. Also, other divalent cations such as Mn^{2+} and Mg^{2+} did not result in aggregation (data not shown) which we conclude is specifically induced by aberrant Zn^{2+}-binding.

mSOD1$^{S\text{-}S}$

The size distribution profile of apo mSOD1$^{S\text{-}S}$ was shown to be monomodal with a mean peak averaging at a hydrodynamic diameter of 4.4±0.15 nm **(Fig. 2B)** which agrees well with the previously determined value of 4.5 nm for the apo monomer[25a].

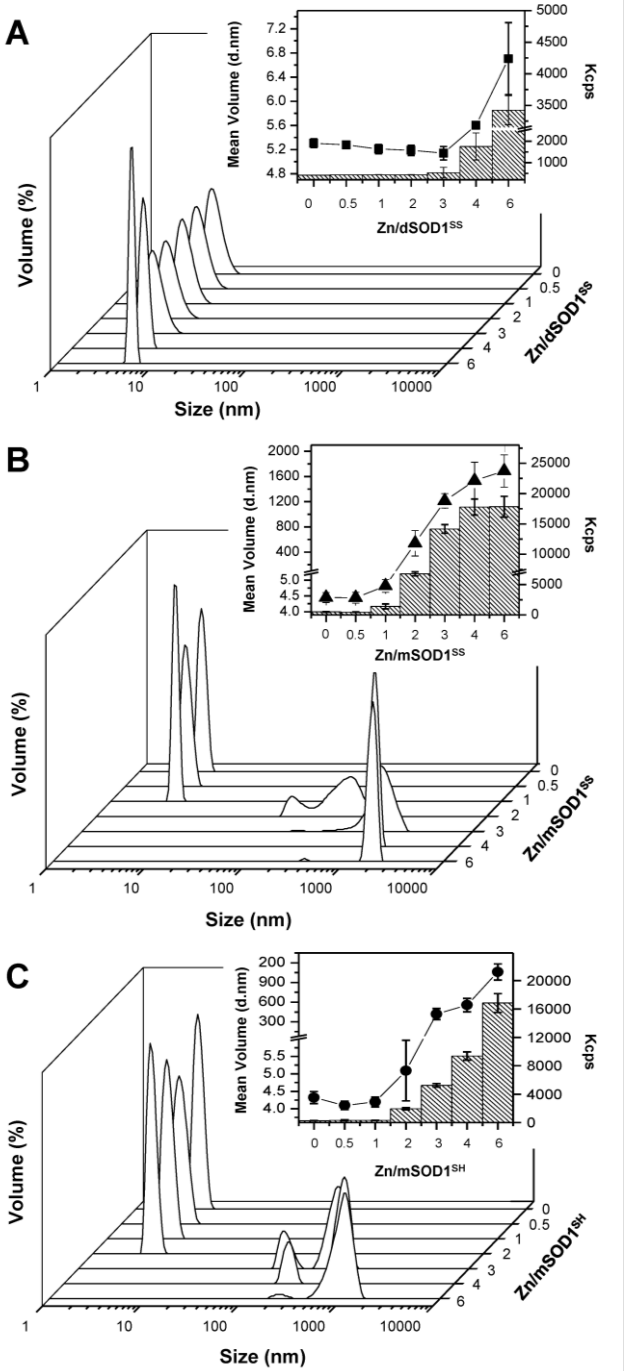

Figure 2. Impact of increasing Zn^{2+} concentration on the size distributions of metal free immature SOD1 conformers. DLS analyses of % volume of dSOD1 $^{S\text{-}S}$ (A), mSOD1 $^{S\text{-}S}$ (B) and mSOD1 ^{SH} (C) at increasing Zn^{2+}/SOD1 ratios up to 6 after 1h of incubation at 37ºC. Inset panels represent the mean volume (d/nm, squares) and mean light scattering intensity (Kcps, bars) at different molar ratios (n=10).

From a molar ratio 2 onwards there is a pronounced increase in the mean light scattering intensity and a multimodal distribution by volume is observed, with the formation of large particles and a corresponding increase in the average hydrodynamic diameter **(Fig. 2B inset)**. Interestingly, molar ratios above 2 results in the formation of even larger aggregate particles and in a higher mean light scattering intensity **(Fig. 2B inset)**. This could be the result of interactions of Zn^{2+} at interfaces that lead to zinc mediated crosslinking and aggregation, as previously proposed[30]. In support of this reasoning is also the observation that Zn^{2+} promotes aggregation of the amyloid β-protein as a result of a crosslinking effect [31] .

mSOD1^{SH}

The size distribution profile of un-metallated mSOD1^{SH} conformer was shown to be monomodal by volume with a mean peak averaging to a hydrodynamic diameter of ≈ 4.3±0.17 nm **(Fig. 2C)**. Thus, the most immature form of apo SOD1 presents the smallest hydrodynamic size of all analyzed conformers, and this agrees well with the fact that this has been the immature form proposed to be capable of efficiently entering the mitochondria[32]. Overall the results obtained when the intramolecular disulfide bridge is reduced are identical to those of the oxidized form, indicating that aggregation is promoted by binding of the second Zn^{2+} **(Fig. 2C, inset)**, irrespective of the redox status of the disulfide bridge. However the significant increase at the highest molar ratios suggesting that interfacial cross linking effects of Zn^{2+} may be more relevant in this conformer than in its oxidized counterpart.

Overall, our results show that all tested conformers become aggregation prone upon non-native binding of Zn^{2+} to SOD1, albeit SOD1 is coordinated with Zn^{2+} to the native zinc-site. This is a very impressive finding, which was so far restricted to SOD1 variant with missing zinc-site ligands in which Zn^{2+} binding to the copper-site renders the protein vulnerable to aggregation, as in ALS-related mutants[33]. Our results however suggest that even with native coordination of Zn^{2+} to the zinc-site, the aggregation features persist. A tempting rationale for this effect is through a reduction on the net charge that would render SOD1 aggregation prone. Indeed this is a mechanism which has been identified in ALS causing SOD1 mutations, which preferentially reduce the repulsive charge of those SOD1 variants[34]. A decrease in net charge is in fact observed for wild type dSOD1$^{S\text{-}S}$ upon zinc binding. In comparison to the metal-free dSOD1$^{S\text{-}S}$, binding of 1 Zn^{2+} increases the protein net charge by 4.0 units and by 3.5 units upon Zn^{2+} binding to all four metal sites in the SOD1 dimer, as experimentally determined by others[35] using protein charge ladders and capillary electrophoresis[35]. Correlation of these observations suggests that, although a decrease in net charge may play an important role, it is clearly not the single mechanism that accounts for our results. These are likely the result of conformational changes resulting from aberrant Zn^{2+} binding that render the SOD1 structure prone to aggregate, and which can be aggravated also by interactions of Zn^{2+} at protein surfaces.

Zn^{2+} binding triggers nucleation independent aggregation

We then investigated the kinetics of Zn^{2+} binding to SOD1 in respect to effects on aggregation at a molar ratio Zn^{2+}/SOD1 of 4. The effect of Zn^{2+} on SOD1 aggregation kinetics was investigated monitoring ThT binding, a fluorescent probe that recognizes cross-β conformations in diverse amyloid-type aggregates (fibrils, amorphous aggregates, oligomers and protofibers)[36].

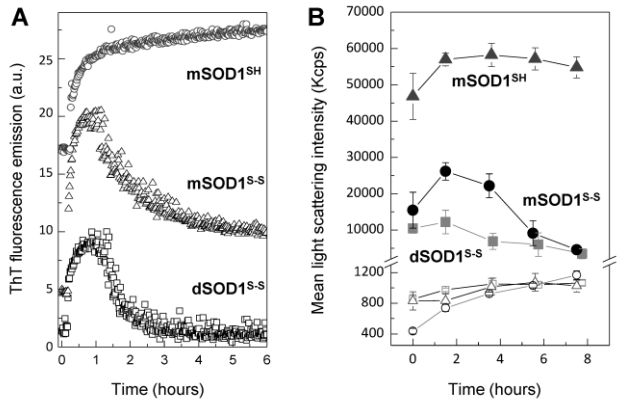

Figure 3. Effect of labile Zn^{2+} in metal free immature SOD1 conformers aggregation. (A) ThT aggregation kinetics of dSOD1^{S-S} (□), mSOD1 $^{S-S}$ (○) and mSOD1 ^{SH} (Δ) at a molar ratio Zn^{2+}/SOD1 of 4. (B) Aggregation profile of SOD1 conformers was monitored by mean light scattering intensity (Kcps) over time, in the absence and in the presence of Zn^{2+} at a molar ratio Zn^{2+}/SOD1 of 4. Open symbols represents SOD1 conformers without zinc and filled symbols represents SOD1 conformers with Zn^{2+}.

We observed that all conformers become ThT reactive within 1 hour upon exposure to Zn^{2+}, which is an indication that Zn^{2+} binding to immature SOD1 results in conformational changes that promote β-sheet stacking (**Fig. 3A**). These conformers are Zn^{2+} specific, as chelation of labile Zn^{2+} with EDTA in a competition experiment results in an inhibition of the aggregation kinetics (**Supplementary Fig. S3**). The absence of a lag phase in the aggregation kinetics suggests that the aggregation mechanism is independent from the formation of aggregation nuclei, which is a priori not favouring fibrillation reactions, in spite of the observed ThT binding. Control experiments in the absence of Zn^{2+} do not evidence the same trend. Curiously, the same kinetic behaviour has been observed in the ALS associated variant SOD1 I113T[37], upon incubation at 37ºC as we have done here. In order to investigate this aspect further, we have used DLS and determined that the initial mean light scattering intensity is highly increased for all SOD1 conformers in respect to controls upon exposure to Zn^{2+} (**Fig. 3B**). This agrees with the formation of amorphous SOD1 aggregates, as discussed in[38]. Indeed, apart from the absence of a lag phase seeding does not influence the kinetic profiles (data not shown). This suggests that intermolecular forces that lead to instantaneous amorphous aggregation occur promiscuously and non-cooperatively.

Following an initial increase in the light scattering, whereas mSOD1SH remains elevated within the next 8h, the dSOD1^{S-S} and mSOD1^{S-S} conformers decay and even reach count values below the ones observed at time zero. A possible explanation for this could be that different types of aggregates are being formed as a function of time, both off-pathway (insoluble aggregation) and on-pathway (conversion into other amyloidogenic precursors). In fact using SDS-PAGE we showed that SOD1 aggregates resulting from Zn^{2+} binding to all SOD1 conformers become less soluble in agreement with the DLS data **(Fig. 4)**.

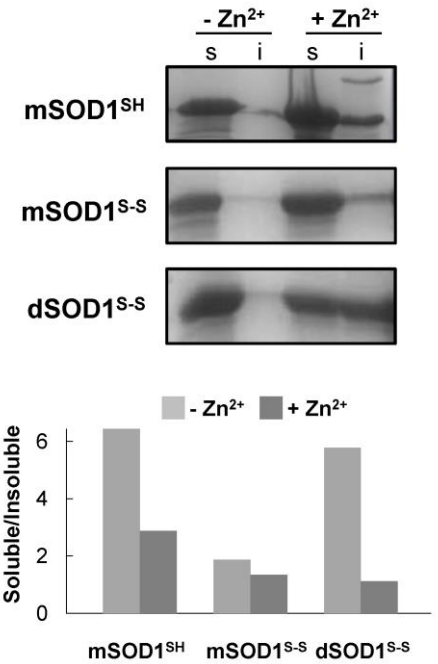

Figure 4. Electrophoretic analysis of soluble versus insoluble SOD1. SOD1 conformers were incubated with and without Zn^{2+}at a Zn^{2+} /SOD1=4 during 14 hours at 37ºC and soluble (s) and insoluble (i) fractions were resolved and analysed by SDS-PAGE (top), and the corresponding soluble:insoluble ratio variations were determined (bottom).

Zn^{2+} binding to SOD1 influences aggregate morphology

We next characterized the morphology of different SOD1 aggregates formed upon Zn^{2+} binding after an 8h reaction at 37°C, using transmission electron microscopy (TEM) and conformational antibodies.

Under the tested conditions, TEM analysis of dSOD1^{S-S} aggregates produced in the absence of Zn^{2+} did not evidence fibrils, although structures resembling amyloidogenic oligomers were visualized (**Fig. 5A**). These species varied in appearance and size and ranged from spherical particles (black arrows) to elongated structures like very short fibrils (black arrowheads). In the presence of Zn^{2+}, the sample was composed of large aggregates, being difficult to confirm if amorphous or presenting any particular structure (**Fig. 5B**).

In contrast, the mSOD1^{S-S} conformer underwent a markedly different behaviour: in this case long mature amyloid fibrils approximately 10 nm wide, were detected (**Fig. 5C**, black arrowhead). mSOD1^{S-S} produced also other fibrillar species and fibrils 5 nm in diameter (white arrow) as well as probable protofilaments. Thicker fibrils, approximately 20 nm wide (black arrow) were also present, and were likely the result of lateral assembly of several 5-nm fibrils. In addition, aggregates and oligomers were also present. For the species generated upon Zn^{2+} binding no such clear fibrillar species were identified and mostly massive aggregates were found (**Fig. 5D**); Similarly to mSOD1^{S-S}, mSOD1^{SH} formed typical amyloid fibrils, approximately 10 nm

in diameter (**Fig. 5E**, arrow). Other species probably aggregates and oligomers were also observed in the vicinity and in contact with fibrils (black arrowheads).

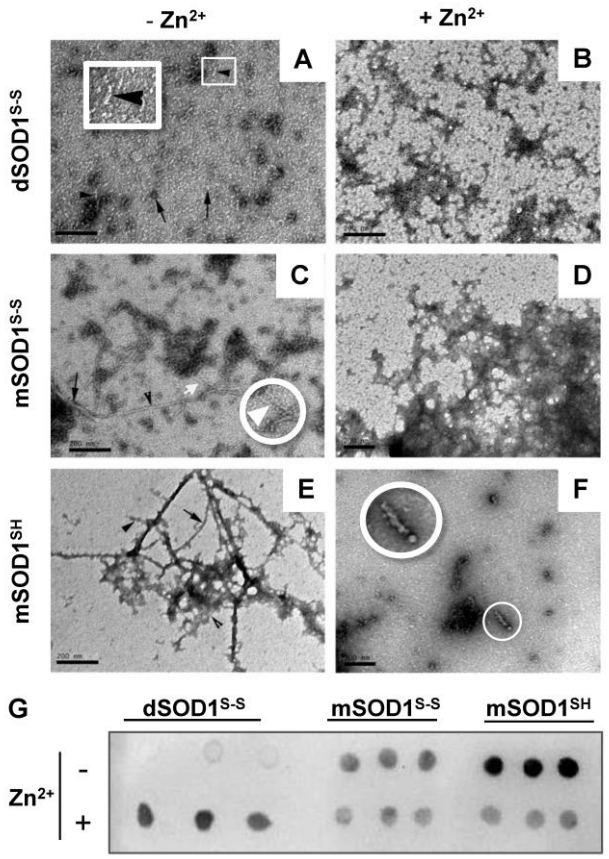

Figure 5. Morphology of SOD1 aggregates. (A-F) TEM images of SOD1 conformers with and without Zn^{2+} with molar ratio Zn^{2+}/SOD1=4, at the plateau phase of ThT aggregation kinetics. Bars equal 200 nm. (G) Dot blot analysis using anti-amyloid fibril (OC) antibody of SOD1 aggregates +/- Zn^{2+}, at the plateau phase of ThT aggregation kinetics (n=3).

Again, binding of Zn^{2+} yields predominantly oligomers and aggregates (**Fig. 5F**). In spite of the amorphous character of SOD1 aggregates formed upon aberrant Zn^{2+} binding, all conformers were reactive for the amyloid specific OC conformational antibody as in[39], albeit at different intensities which cannot be particularly valued in this type of qualitative dot-blot (**Fig. 5G**).

To determine if the aggregates produced in the presence of Zn^{2+} result in prototypic fibrillar structures or contain seed-competent conformations that result in fibril formation in longer time scales, we have also carried out a combined imaging and electron diffraction analysis of aged SOD1 aggregates. Indeed, it has been previously established that the kinetics of metal-free SOD1 aggregation, performed in conditions identical to ours, only reaches the plateau phase after 4 months of incubation[6a]. Upon incubation for 6 months, a range of different morphologies was observed (**Fig. 6 and Table 2**). The most common patterns were clusters of oval or slate-like protein aggregates that were often in contact to branching material and clusters of single fibrils that appeared like tufts of hair (as in Fig. 5E). Needles and single fibrils without contact to other material were also frequently observed (**Fig. 6**). The fibrils had net diameters of 10-30 nm. The size of the single fibrils is in accordance with earlier findings[40] showing 10 nm thick single SOD1 fibrils and aggregates of two or more fibrils with net diameter of about 15-25 nm.

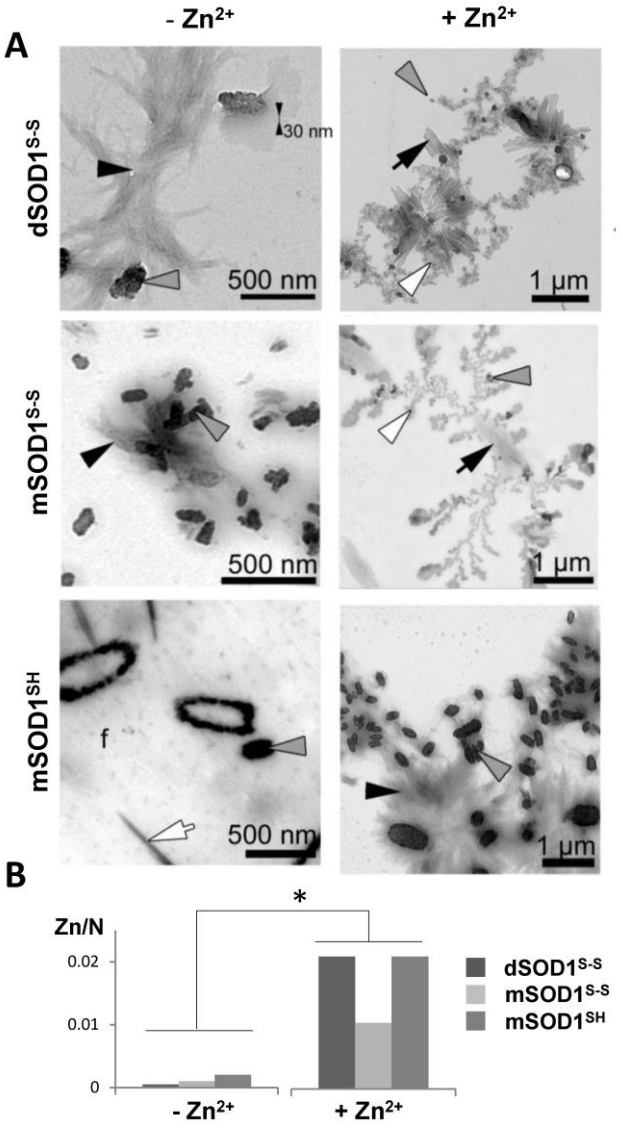

Figure 6. Electron microscopy micrographs of unstained aged aggregates of SOD1 conformers (A). $dSOD1^{S-S}$, $mSOD1^{S-S}$ and $mSOD1^{SH}$ - with and without Zn^{2+}, with molar ratio Zn^{2+}/SOD1=4: oval (grey arrow head) or slate-like (black arrow) shaped material or hair (black arrow head) were common in all samples and increased with Zn^{2+}. Branch-like (white arrow head) material or needles (white arrow) were observed less frequently. See Table 2 for qualitative quantification of morphologies. (B) Zn/N ratios of SOD1 aged aggregates with and without Zn^{2+} at a molar ratio Zn^{2+}/SOD1=4, calculated after performed EDX and EELS analysis to aged SOD1 conformers aggregates. N stands for nitrogen as a marker for SOD proteins. Samples without Zn^{2+} contain Zn^{2+} are at the detection limit. P-value<0.0001 concerning the differences observed + Zn^{2+}/- Zn^{2+}.

Stacked fibres had been observed at the earlier stages of aggregation (**Fig. 5c**) and likely lead to the slate-like

morphologies as a result of lateral assembly. It is particularly noteworthy that oval (grey arrow head) or slate-like (black arrow) shaped materials or hair-like (black arrow head) seem to accumulate in the aggregates formed in the presence of Zn^{2+} (**Fig. 6A, Table 2**).

Table 2 - Qualitative analysis of the morphologies of aged SOD1 aged aggregates [a]

		Morphology [a]					
		Hair, stars	**Single fibrils**	**Needle**	**Branch**	**Oval**	**Slate**
dSOD1^{SS}	- Zn^{2+}	+++	+++	-	+++	-	++
	+ Zn^{2+}	+	+++	-	+++	++	+++
mSOD1^{SS}	- Zn^{2+}	+	++	++	-	++	++
	+ Zn^{2+}	+	++	++	+	++	++
mSOD1^{SH}	- Zn^{2+}	+	+	+	+++	++	+
	+ Zn^{2+}	+++	+	-	+	++	+++

[a] The diffraction patterns of SOD1S-S, mSOD1S-S and mSOD1SH with and without Zn^{2+} at a molar ratio of Zn^{2+}/SOD1=4 were accessed to obtain this qualitative analysis of the different types of observed morphologies. .- None;+ some; ++ moderate; +++ abundant structures in the sample.

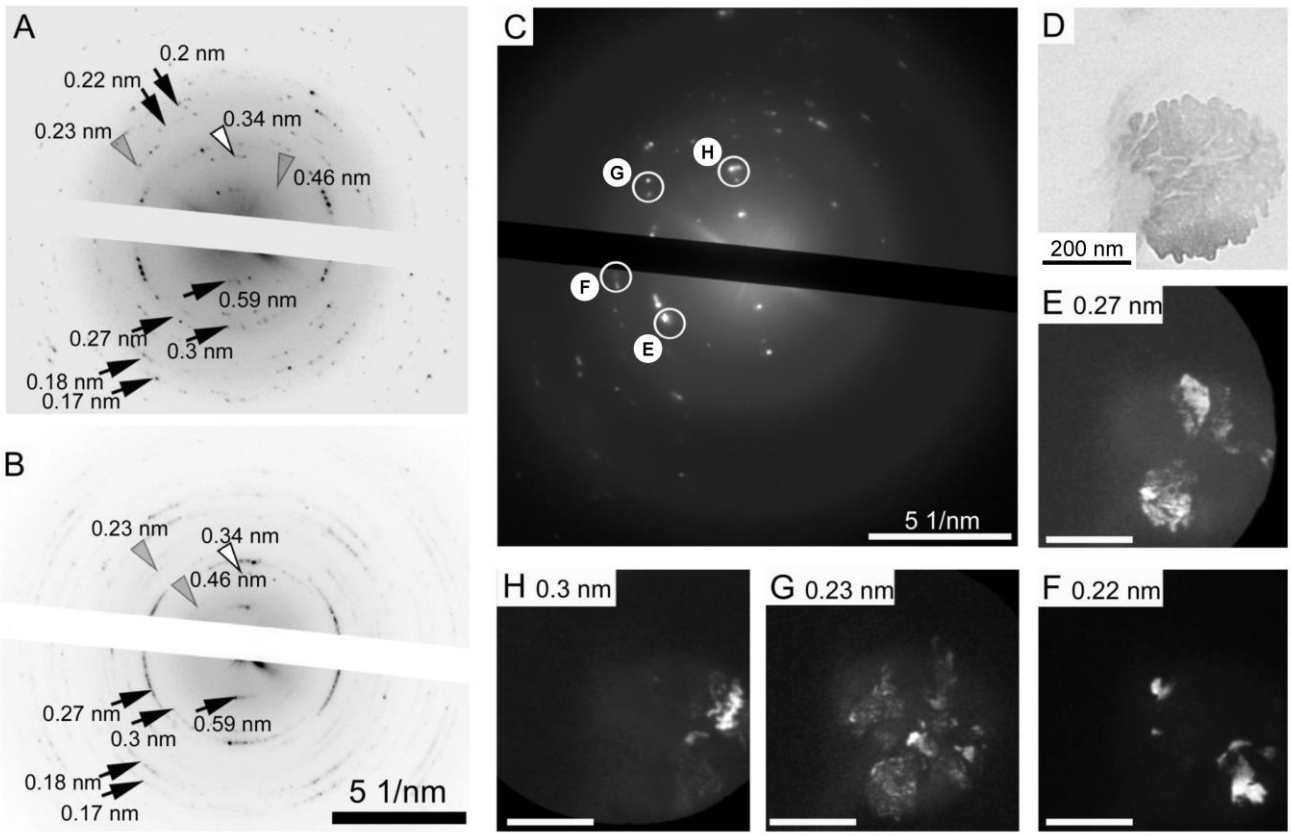

Figure 7. Electron diffraction analysis of aged dSOD1^{S-S} aggregates. (A-B) Electron diffraction patterns of aged dSOD1^{S-S} aggregates with (A) and without Zn^{2+} (B) with molar ratio Zn^{2+}/SOD1=4. Main reflections (black arrows) between 0.27 nm and 0.3 nm (second order) and at about 0.59 nm (first order); weaker reflections at 0.34 nm (white arrow); grey arrow heads label the 0.43 nm and 0.23 nm reflection rings. (C) Bright field image corresponding to the diffraction pattern in A and dark field images (E-H): Each reflection ring of the diffraction pattern corresponds to a certain structure in the dSOD1SS aggregate that can be visualized by dark field imaging. The reflection at 0.23 nm (G) corresponds to the amyloid-like misfolded proteins. Note the area highlighted in (H) shows a single protein fibril of about 10 nm thickness curled up in the protein matrix. See "Materials and Methods" for further details.

We have then used Energy-dispersive X-ray microanalysis (EDX) and Electron energy loss spectroscopy (EELS) to determine if Zn^{2+} remains bound to SOD1 aggregated. After extensive dialysis of aged SOD1 aggregates to remove all labile Zn^{2+}, combined EDX-EELS analyses were used to acquire Zn/N ratios which yielded the ratio of protein (as determined by N content) compared to that of Zn (**Fig. 6B**). The statistics of the Zn/N ratios concerning samples with and without Zn^{2+} are valuable ($p < 0.0001$) showing that a higher fraction of Zn^{2+} is incorporated and remains bound in aged SOD1 aggregates. Nevertheless, this ratio is low (**Fig. 6B**), indicating that zinc dissociates during the aging process.

Electron diffraction analysis of SOD1 aggregates

To have further structural and morphological information on these aged SOD1 aggregates we used electron diffraction analysis. For this purpose and to gain enough signal, only larger aggregates (such as the oval and slate-like materials) were investigated. For all cases we observed diffraction spots arranged in rings in which the diameter of the ring directly relates to the lattice spacing of the crystalline phase (**Fig. 7AB**). Thus, the observed presence of reflection spots is a direct proof of the presence of nano-scaled crystalline materials (see also supplementary **Fig. S4**).

We compared the obtained electron diffraction patterns with those of cross-β conformations characteristic of amyloids, which yield reflections at 0.23 nm, 0.47 nm and 1.1 nm d-spacing[41]. We observed such amyloid-type patterns in SOD1 aggregates, namely the first order 0.46 nm reflection and its corresponding second order 0.23 nm reflections (**Fig. 7AB**, grey arrows). In spite of some variations in intensity, no clear correlations can be established between aggregates produced with and without zinc: the 0.23 nm diffraction appears generally as more intense in the zinc-free samples, but they are however both relatively weak (supplementary **Table S2**). In general, reflections with values higher than 0.6 nm could not be evaluated due to high central background, so the other cross-β 1.1 nm reflection could not be observable. In addition, we detect a triple band of reflections between 0.27 nm and 0.3 nm d-spacing and their first order corresponding partner reflections at about 0.59 nm d-spacing (**Fig. 7AB**, black arrows). Another unassigned weaker reflection at 0.34 nm was also present, frequently as a single reflection (white arrow head), which seems less intense in some zinc-free samples (supplementary **Table S2**). These additional reflections are probably an indication of variations around the maxima inter- and intra- β-sheet distances, which is a known feature in amyloid aggregates[42], as well as in SOD1 amyloidogenic aggregates, which have been proposed to be structurally polymorphic[43].

We further collected dark field images at different electron reflection signals of $dSOD1^{S\text{-}S}$ with Zn^{2+}, to show the different areas of the protein that relate to the reflections (**Fig. 7 c-h**). The area responsible for the amyloid-like reflection at 0.23 nm d-spacing was analysed (**Fig. 7g**), and the spots in the electron diffraction pattern indicate the presence of single microcrystals, which cover a high portion of the protein area visible in the bright field image (**Fig. 7d**). Note that the hair-like material on the left does not participate in the diffraction signal. The apertures were localized around a few diffracted beams for the dark field images so that some of the microcrystals appear with bright contrast, namely those whose diffracted beams partly pass the objective aperture. Again, the observed nano-aggregates have rather heterogeneous and polymorphic structures, which include clustered, scattered but also fibrillar aggregates. In fact, a single protein fibril with about 10 nm diameter is observed (**Fig. 7h**).

Conclusions

Here we provide evidence that aberrant zinc binding to immature conformers of metal-free copper-zinc SOD1 triggers the formation of amorphous aggregates, a finding with potential relevance to understand the formation of pathologic SOD1 aggregates in ALS. We show that Zn^{2+} binding to the zinc site is not by itself triggering this process; rather, Zn^{2+} binding to other SOD1 sites such as the copper-site and interfacial residues at the protein surface triggers nucleation independent aggregation.

The analysis of the aggregates formed at different stages of the aggregation process indicates a wide range of morphologies, an observation which finds a parallel with the SOD1 inclusions found in ALS which are also biophysically and morphologically heterogeneous[44]. Considering the fact that Zn^{2+} is upregulated in ALS affected motor neurons we posit that such aberrant zinc-protein interactions may take place in cells and be one of the factors contributing to the onset of SOD1 pathological aggregation. Nevertheless, due to the relatively low affinity of the copper-site for Zn^{2+}, this would require a severe dysfunction of the pool of labile Zn^{2+}. We thus propose a model for the effects of aberrant zinc-binding on SOD1 aggregation (**Fig. 8**) that conciliates our observations with the previously reported high structural polymorphism of SOD1 aggregates[43]. The previous crystal structure of the Zn/Zn SOD1 conformer was found to be identical to that of the Cu/Zn protein, except at the copper-site[45]. Our data suggests that zinc overload and aberrant coordination likely result in an altered breathing dynamics and higher misfolding propensity. Indeed, it is very interesting to note that the same happens with ALS associated variants (such as SOD1 D76V, D101N and N139K) which have stabilities and folding properties which are nearly indistinguishable from those of wild type SOD1[46] but actually present an increased propensity to aggregate [47].

Cite this: DOI: 10.1039/c0xx00000x

www.rsc.org/xxxxxx

Paper

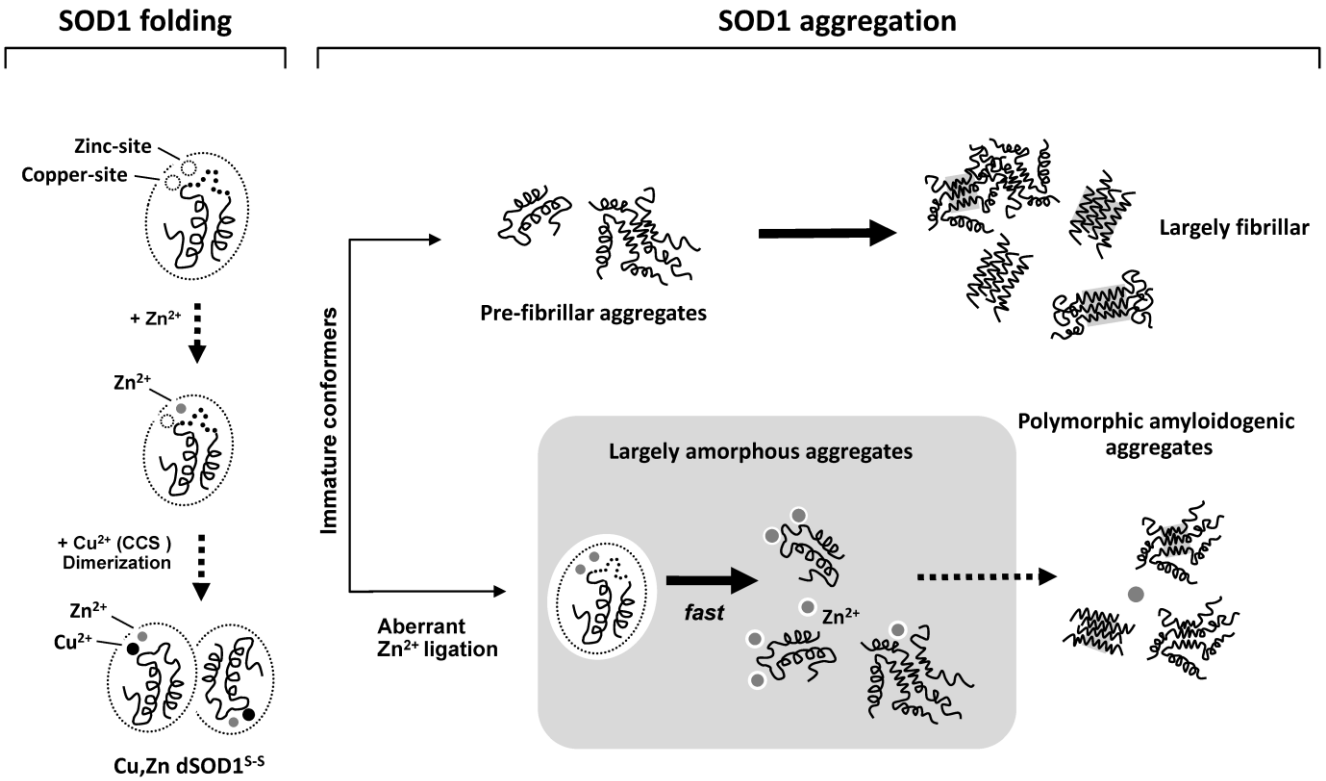

Figure 8. Schematic representation for the effects of aberrant zinc-binding on SOD1 aggregation.The scheme illustrates the native folding (left) and aggregation pathways (right) of SOD1. SOD1 folding proceeds through stepwise insertion of Zn^{2+} (via yet unknown mechanisms) and Cu^{2+} (via the CSS chaperone) and dimerization. Immature metal-free conformers are the likely precursors of aggregation pathways that result in the formation toxic protein aggregates in ALS. Aberrant Zn^{2+} coordination under metal dyshomeostatic conditions favours the fast formation of largely amorphous zinc-induced aggregates that evolve to polymorphic amyloidogenic aggregates with time. See text for further details.

Experimental

Chemicals and Proteins

All reagents were of the highest grade commercially available. All solutions and buffers were passed through a chelex resin (Bio-Rad) column to remove contaminant trace metals.

SOD1 Purification

$dSOD1^{S-S}$ was expressed in *E. coli* BL21(DE3) cells and purified as in [48]. All experiments were performed with the demetallated $dSOD1^{S-S}$ form, obtained accordingly with previous published protocols[7b]. The concentration of $dSOD1^{S-S}$ was determined spectrophotometrically using the extinction coefficient 10800 $cm^{-1}M^{-1}$ at 280nm.

$mSOD1^{S-S}$ was studied using the mutant SOD1-F50E/G51E and was expressed in *E. coli* BL21(DE3) cells and purified with a His-binding column (HisTrap HP 5mL, GE Healthcare). The protein was incubated overnight with TEV protease (containing a His tag) in a digestion Buffer (3 mM Glutathione/0.3 mM Oxidized glutathione, 10 µM ZnCl, 200 mM NaCl, 5 mM Citrate and 20 mM TRIS-HCl pH 7.4) to cleave the histidine tag. The two proteins were loaded in a His-binding column followed by a Superdex 75 gel filtration (GE Healthcare). The concentration of $mSOD1^{S-S}$ was determined spectrophotometrically using the extinction coefficient 5500 $cm^{-1}M^{-1}$ at 280nm. $mSOD1^{SH}$ was prepared adding 5 mM tris(2-carboxyethyl)phosphine (TCEP) and incubating 1h.

Isothermal titration calorimetry

The interaction of Zn^{2+} with SOD1 conformers - $dSOD1^{S-S}$, $mSOD1^{S-S}$, $mSOD1^{SH}$ - was analyzed using isothermal titration calorimetry (ITC) on a Microcal ITC 200 calorimeter. This study was performed at pH 7.4 and 37ºC in order to mimic physiological conditions, and to prevent high affinity binding to the zinc-site, which is known to be favoured by more acidic conditions[7b, 49]. Titrations were performed at 37ºC by injecting 1µl aliquots of a $ZnCl_2$ solution (400 µM) into non metallated SOD1 conformers (80 µM) in the sample cell. Each injection was made with a 140 s spacing interval between subsequent thirty

eight injections with stirring at 1000 rpm. Apo SOD1 conformers were previously extensively dialyzed against 50 mM TRIS pH 7.5. The apo SOD1-metal ion titration curves were corrected using a Zn^{2+} to buffer control titration. In order to provide more data points and drive Zn^{2+} titration on apo SOD1 to saturation, three sequential ITC titrations were merged with the program ConCat32. Before the beginning of each sequential ITC titration the excess solution was removed from the overflow reservoir and the same $ZnCl_2$ solution was used in all three titrations. Data were analysed using the non-linear regression analyses of a multiple binding site model with up to four overlapping binding equilibrium provided in [21].

Dynamic Light Scattering

Dynamic light scattering (DLS) measurements were carried out in a Malvern Zetasizer nano ZS instrument, equipped with a 4-megawatt He-Ne laser (632 nm). Samples were centrifuged 5 min at 15000x g and filtered through a 0.45-µm filter into a 3-mm light path quartz cuvette (Hellma) prior to analysis. SOD1 conformers (50 µM in 50 mM TRIS pH 7.4) were analyzed at different molar ratios of Zinc (0; 0.5; 1; 2; 3 and 4 Zn^{2+}/SOD1), after 1h of incubation at 37 ºC. For aggregation kinetics 150 µM of SOD1 samples were used and incubated at 37ºC without agitation. After 1.5; 3.5; 5.5 and 7.5 h of incubation 50 µl of aliquots were collected and measured. The operating procedure was set to 8 runs. Data were analyzed by using DTS software (Version 6.32, Malvern) in respect to the distribution of sizes by volume, Z-average (Z-agg) and derived count rate (Kcps). For the seeding experiments, SOD1 samples were incubated at a ratio of Zn:SOD1=4 for 1.5 hours at room temperature, to promote the formation of aggregates. Seeding reactions were done by adding 10% of these Zn induced aggregates (5µM) to apo SOD1 solution (50µM). SOD1 aggregation was monitored by DLS at 37ºC during a period of 8 hours.

Thioflavin T Fluorescence Binding

Real time ThT fluorescence emission at 480 nm was recorded using a Cary Varian Eclipse instrument, equipped with a Peltier temperature control set for all measurements at 37 °C, upon excitation at 440nm. Aggregation assays were performed with 150 µM of SOD1 samples ($dSOD1^{S\text{-}S}$, $mSOD1^{S\text{-}S}$, $mSOD1^{SH}$) then adding $ZnCl_2$ in a molar ratio of Zn^{2+}/SOD1=4 after 10 min. 2 molar ratio of ThT in 50mM TRIS, pH 7.4 was also added to the solutions.

Evaluation of insoluble aggregates by SDS PAGE

The levels of soluble and insoluble aggregates were analyzed using 12% SDS-PAGE. 200 µl of 150 µM of SOD1 samples ($dSOD1^{S\text{-}S}$, $mSOD1^{S\text{-}S}$, $mSOD1^{SH}$) were incubated 14 h at 37ºC, 260 rpm with and without zinc ions (molar ratio of Zn^{2+}/SOD1=4). The samples were centrifuged 45 min at 15000x g to separate the insoluble fraction from the total fraction. After centrifugation, the supernatants (soluble aggregates and soluble protein) were transferred to a fresh tube and precipitated with 15% of Trichloroacetic Acid (TCA). The samples were incubated 15 min and centrifuged 30 min at 15000x g. Both pellets were resuspended in loading buffer. The absolute intensity of each band was quantified using Image Lab (Biorad).

Transmission Electron Microscopy

5 µl of 150 µM of different conformers of SOD1 ($dSOD1^{S\text{-}S}$, $mSOD1^{S\text{-}S}$, $mSOD1^{SH}$) with and without a molar ratio of Zn^{2+}/SOD1=4 were obtained at the plateau phase of ThT aggregation kinetics. The samples were absorbed to carbon-coated collodion film supported on 400-mesh copper grids and negatively stained with 1% uranyl acetate. The grids were exhaustively visualized with a Jeol microscope (JEM-1400), operated at 80 kV. (In aged SOD samples, EM was performed on formvar-coated Al-grids and without UAC staining).

Dot-Blot analysis

10 µl of SOD1 aggregates obtained at the plateau phase of each ThT aggregation kinetic curve were dotted in triplicates onto PVDF membranes and probed with a 1:1000 for the anti-amyloid fibril OC antibody (AB2286, Merck Millipore) according to the manufacturer's instructions. Dots were visualized using a horseradish peroxidase-conjugated IgG secondary antibody with a chemiluminescence detection system (GE Healthcare). Images were recorded and analyzed using Quantity One analysis software from Bio-Rad.

Energy-dispersive X-ray microanalysis (EDX) and Electron energy loss spectroscopy (EELS)

150 µM SOD1 samples ($dSOD1^{S\text{-}S}$, $mSOD1^{S\text{-}S}$, $mSOD1^{SH}$) were incubated with and without Zn (molar ratio of Zn^{2+}/SOD1=4) for 200 minutes and dialyzed overnight with 50 mM TRIS pH 7.4 to remove excess of zinc ions in solution. Aging samples of these SOD1 aggregates obtained at the plateau phase of each ThT aggregation kinetic curve were diluted prior to EM analysis with ddH2O (1:1000) and 5 µl of that dilution were immediately dropped on a formvar-coated 100 mesh aluminum grid (Plano GmbH, Wetzlar, Germany) and dried under a clean bench to avoid dust contamination. No further contrast enhancement like staining with osmiumtetroxide, uranylacetate or lead citrate was performed to avoid artefacts in the chemical analyses. The samples were investigated under a Zeiss 912 Omega transmission electron microscope (TEM) equipped with an energy filter, CCD camera (2kx2k) and an EDX detector with an ultrathin window and a digital pulse processor for chemical analysis (See below) at magnifications ranging from 1800x – 140000x.

Chemical analysis in the TEM was performed as described elsewhere [50]. Energy-dispersive X-ray microanalysis (EDX) and Electron energy loss spectroscopy (EELS) were performed at individual areas of the same protein spots at a magnification of 12500x using thinner edges for EELS and thicker central areas for EDX.

A special stray aperture was used and the sample was mounted on top of the grid always facing the EDX detector to keep stray radiation to a minimum. EDX spectra were acquired with a 100 nm spot for at least 200 seconds and were quantitatively analyzed by the INCA software (INCA, 2001) using the standardless Cliff–Lorimer k-factor method. The same k-factors as in [51] were used. They yielded spectra with >100 000 nettocounts for C permitting a minimum detectable mole fraction of 0.02 at % Zn (= 0.1 wt% Zn).

EELS acquisition and data analysis were performed using the Esivision software (Esivision, 2002). The smallest objective aperture (3.5 mrad) was used for bright-field imaging and low loss EELS, a medium objective aperture (8mrad) was used for acquiring core-loss EELS of C–K and N–K ionization edges. The

local section thickness was determined by low-loss EELS. EELS core loss spectra including the C and N ionization edge were quantified by using a 30 eV window, integrating the net counts of the ionization edges and using calculated ionization cross sections to determine mole fraction ratios of C/N with a detection limit of less than 0.4 at% N. The cN/cC mole fraction ratio as determined by EELS was then used to recalculate all mole fractions determined by EDX by dividing them by (1 + cC (cN/cC)), i.e. by (1 + ab), a being the carbon mole fraction determined by EDX and b being (cN/cC) determined by the EELS quantitative analysis. The EELS spectra at the N-K ionization edge had about 1500 counts yielding a MDMF of N of 0.4 at%. No corrections were applied to the individual spectra, e.g. no absorption correction for EDX and no spectrum deconvolution for EEL spectra for accounting for multiple inelastic scatterings.

Electron diffraction analysis

The microscope was operated at 120 kV. A detailed camera calibration was carried out prior to acquisition. Regions of interest were investigated in the imaging mode at 10000x-63000x magnification. A selected area diffraction aperture with a diameter of 800 nm was inserted, and an energy slit aperture of 5 eV used, then the microscope was switched into the diffraction mode and protein spots were investigated at a camera length of 290 mm - 900 mm. Diffraction patterns were acquired with a highly parallel beam (maximum divergence of about 0.2 mrad) for about 20 s acquisition time. The intensity of the diffraction spots originating from protein crystals were clearly identified on top of the central background if larger than 3.4 nm^{-1}. (max. 0.6 nm d-spacing). Diffraction spots were arranged in rings and the diameter of the ring directly relates to the lattice spacing of the crystalline phase. Thus, the presence of reflection spots is a direct proof of nano-scaled crystalline material. For dark field imaging, the objective aperture was inserted and aligned to certain diffraction spots as indicated in the Figure legends.

Abbreviations

ALS, Amyotrophic lateral sclerosis
DLS, Dynamic light scattering
EELS, electron energy-loss spectroscopy
EDX, energy-dispersive X-ray spectroscopy
ITC, Isothermal titration calorimetry
SOD1, Superoxide dismutase 1
TEM, Transmission electron microscopy
ThT, Thioflavin-T

Acknowledgements

This work was supported by the Fundação para a Ciência e Tecnologia (FCT/MCTES, Portugal) through: research grants PTDC/QUI-BIQ/117789/2010 (to CMG), post-doctoral fellowship SFRH/BPD/47477/2008 to SSL, and by the strategic grant PEst-OE/EQB/LA0004/2011 (to the ITQB Laboratório Associado). We gratefully acknowledge J.S. Valentine (University California Los Angeles) for comments on the manuscript, M. Oliveberg (Stockholm University) for the dSOD1 expression plasmid and P. John Hart (Texas University) for the mSOD1 expression plasmid. We thank Ulrich Schraermeyer (Core Facility for Electron Microscopy, University Hospital Tuebingen) and Oliver Eibl (Institute of Applied Physics, University of Tuebingen) and for great help and discussion of the electron diffraction analyses on the manuscript. CMG and AB would like to acknowledge networking support by the COST Action TD1304 - The Network for the Biology of Zinc (Zinc-Net).

Notes and references

[a] *Instituto Tecnologia Química e Biológica, Universidade Nova de Lisboa, Oeiras, Portugal. Fax: +351-214411277; Tel: +351-214469332; leal@itqb.unl.pt; jcristovao@itqb.unl.pt; gomes@itqb.unl.pt*
[b] *Center for Ophthalmology and Core Facility for Electron Microscopy at the University Hospital, University of Tubingen, Germany. Fax: +49-7071294554; Tel: +49-70712984774; E-mail: antje.biesemeier@uni-tuebingen.de*
[c] *Modulation in Neurodegenerative Disorders (MiND group), Instituto de Biologia Molecular e Celular, Porto, Portugal. Fax: +351-226099157; Tel: +351-226074900; E-mail: icardoso@ibmc.up.pt*

‡ *Equally contributing authors*
* *Corresponding author (Cláudio M. Gomes, gomes@itqb.unl.pt)*

† Electronic Supplementary Information (ESI) available

1. (a) K. Asayama, I. M. Burr, Rat superoxide dismutases. Purification, labeling, immunoassay, and tissue concentration. *J Biol Chem* 1985, *260*. 2212-7; (b) C. A. Pardo, Z. Xu, D. R. Borchelt, D. L. Price, S. S. Sisodia, D. W. Cleveland, Superoxide dismutase is an abundant component in cell bodies, dendrites, and axons of motor neurons and in a subset of other neurons. *Proc Natl Acad Sci U S A* 1995, *92*. 954-8.

2. (a) L. P. Rowland, N. A. Shneider, Amyotrophic lateral sclerosis. *N Engl J Med* 2001, *344*. 1688-700; (b) E. Kabashi, P. N. Valdmanis, P. Dion, G. A. Rouleau, Oxidized/misfolded superoxide dismutase-1: the cause of all amyotrophic lateral sclerosis? *Ann Neurol* 2007, *62*. 553-9; (c) A. Gruzman, W. L. Wood, E. Alpert, M. D. Prasad, R. G. Miller, J. D. Rothstein, R. Bowser, R. Hamilton, T. D. Wood, D. W. Cleveland, V. R. Lingappa, J. Liu, Common molecular signature in SOD1 for both sporadic and familial amyotrophic lateral sclerosis. *Proc Natl Acad Sci U S A* 2007, *104*. 12524-9; (d) M. S. Rotunno, D. A. Bosco, An emerging role for misfolded wild-type SOD1 in sporadic ALS pathogenesis. *Front Cell Neurosci* 2013, *7*. 253, DOI: 10.3389/fncel.2013.00253; (e) K. Forsberg, P. M. Andersen, S. L. Marklund, T. Brannstrom, Glial nuclear aggregates of superoxide dismutase-1 are regularly present in patients with amyotrophic lateral sclerosis. *Acta Neuropathol* 2011, *121*. 623-34, DOI: 10.1007/s00401-011-0805-3; (f) Y. Furukawa, Pathological roles of wild-type cu, zn-superoxide dismutase in amyotrophic lateral sclerosis. *Neurol Res Int* 2012, *2012*. 323261, DOI: 10.1155/2012/323261; (g) S. Guareschi, E. Cova, C. Cereda, M. Ceroni, E. Donetti, D. A. Bosco, D. Trotti, P. Pasinelli, An over-oxidized form of superoxide dismutase found in sporadic amyotrophic lateral sclerosis with bulbar onset shares a toxic mechanism with mutant SOD1. *Proc Natl Acad Sci U S A* 2012, *109*. 5074-9, DOI: 1115402109 [pii] 10.1073/pnas.1115402109.

3. (a) L. J. Hayward, J. A. Rodriguez, J. W. Kim, A. Tiwari, J. J. Goto, D. E. Cabelli, J. S. Valentine, R. H. Brown, Jr., Decreased metallation and activity in subsets of mutant superoxide dismutases associated with familial amyotrophic lateral sclerosis. *J Biol Chem* 2002, *277*. 15923-31, DOI: 10.1074/jbc.M112087200

M112087200 [pii]; (b) J. A. Rodriguez, J. S. Valentine, D. K. Eggers, J. A. Roe, A. Tiwari, R. H. Brown, Jr., L. J. Hayward, Familial amyotrophic lateral sclerosis-associated mutations decrease the thermal stability of distinctly metallated species of human copper/zinc superoxide dismutase. *J Biol Chem* 2002, *277*. 15932-7, DOI: 10.1074/jbc.M112088200

M112088200 [pii]; (c) D. Bordo, K. Djinovic, M. Bolognesi, Conserved patterns in the Cu,Zn superoxide dismutase family. *J Mol Biol* 1994, *238*. 366-86, DOI: S0022-2836(84)71298-8 [pii]

10.1006/jmbi.1994.1298.

4. (a) R. W. Strange, S. Antonyuk, M. A. Hough, P. A. Doucette, J. A. Rodriguez, P. J. Hart, L. J. Hayward, J. S. Valentine, S. S. Hasnain, The structure of holo and metal-deficient wild-type human Cu, Zn superoxide dismutase and its relevance to familial amyotrophic lateral sclerosis. *J Mol Biol* 2003, *328*. 877-91; (b) L. Banci, I. Bertini, F. Cramaro, R. Del Conte, M. S. Viezzoli, Solution structure of Apo Cu,Zn superoxide dismutase: role of metal ions in protein folding. *Biochemistry* 2003, *42*. 9543-53, DOI: 10.1021/bi034324m; (c) M. Assfalg, L. Banci, I. Bertini, P. Turano, P. R. Vasos, Superoxide dismutase folding/unfolding pathway: role of the metal ions in modulating structural and dynamical features. *J Mol Biol* 2003, *330*. 145-58, DOI: S0022283603005333 [pii].

5. (a) Y. Furukawa, T. V. O'Halloran, Posttranslational modifications in Cu,Zn-superoxide dismutase and mutations associated with amyotrophic lateral sclerosis. *Antioxid Redox Signal* 2006, *8*. 847-67, DOI: 10.1089/ars.2006.8.847; (b) A. Hornberg, D. T. Logan, S. L. Marklund, M. Oliveberg, The coupling between disulphide status, metallation and dimer interface strength in Cu/Zn superoxide dismutase. *J Mol Biol* 2007, *365*. 333-42, DOI: S0022-2836(06)01272-1 [pii]

10.1016/j.jmb.2006.09.048.

6. (a) L. Banci, I. Bertini, A. Durazo, S. Girotto, E. B. Gralla, M. Martinelli, J. S. Valentine, M. Vieru, J. P. Whitelegge, Metal-free superoxide dismutase forms soluble oligomers under physiological conditions: a possible general mechanism for familial ALS. *Proc Natl Acad Sci U S A* 2007, *104*. 11263-7, DOI: 10.1073/pnas.0704307104; (b) M. J. Lindberg, L. Tibell, M. Oliveberg, Common denominator of Cu/Zn superoxide dismutase mutants associated with amyotrophic lateral sclerosis: decreased stability of the apo state. *Proc Natl Acad Sci U S A* 2002, *99*. 16607-12, DOI: 10.1073/pnas.262527099

262527099 [pii]; (c) C. M. Karch, M. Prudencio, D. D. Winkler, P. J. Hart, D. R. Borchelt, Role of mutant SOD1 disulfide oxidation and aggregation in the pathogenesis of familial ALS. *Proc Natl Acad Sci U S A* 2009, *106*. 7774-9, DOI: 0902505106 [pii]

10.1073/pnas.0902505106; (d) Y. Furukawa, K. Kaneko, K. Yamanaka, T. V. O'Halloran, N. Nukina, Complete loss of post-translational modifications triggers fibrillar aggregation of SOD1 in the familial form of amyotrophic lateral sclerosis. *J Biol Chem* 2008, *283*. 24167-76, DOI: M802083200 [pii]

10.1074/jbc.M802083200.

7. (a) L. Leinartaite, K. Saraboji, A. Nordlund, D. T. Logan, M. Oliveberg, Folding catalysis by transient coordination of Zn2+ to the Cu ligands of the ALS-associated enzyme Cu/Zn superoxide dismutase 1. *J Am Chem Soc* 2010, *132*. 13495-504, DOI: 10.1021/ja1057136; (b) S. Z. Potter, H. Zhu, B. F. Shaw, J. A. Rodriguez, P. A. Doucette, S. H. Sohn, A. Durazo, K. F. Faull, E. B. Gralla, A. M. Nersissian, J. S. Valentine, Binding of a single zinc ion to one subunit of copper-zinc superoxide dismutase apoprotein substantially influences the structure and stability of the entire homodimeric protein. *J Am Chem Soc* 2007, *129*. 4575-83; (c) L. Banci, I. Bertini, F. Cantini, M. D'Onofrio, M. S. Viezzoli, Structure and dynamics of copper-free SOD: The protein before binding copper. *Protein Sci* 2002, *11*. 2479-92, DOI: 10.1110/ps.0210802; (d) C. Kayatekin, J. A. Zitzewitz, C. R. Matthews, Zinc binding modulates the entire folding free energy surface of human Cu,Zn superoxide dismutase. *J Mol Biol* 2008, *384*. 540-55, DOI: S0022-2836(08)01189-3 [pii]

10.1016/j.jmb.2008.09.045.

8. L. Banci, I. Bertini, F. Cantini, T. Kozyreva, C. Massagni, P. Palumaa, J. T. Rubino, K. Zovo, Human superoxide dismutase 1 (hSOD1) maturation through interaction with human copper chaperone for SOD1 (hCCS). *Proc Natl Acad Sci U S A* 2012, *109*. 13555-60, DOI: 1207493109 [pii]

10.1073/pnas.1207493109.

9. L. Banci, L. Barbieri, I. Bertini, F. Cantini, E. Luchinat, In-cell NMR in E. coli to monitor maturation steps of hSOD1. *PLoS One* 2011, *6*. e23561, DOI: 10.1371/journal.pone.0023561

PONE-D-11-08035 [pii].

10. L. Banci, L. Barbieri, E. Luchinat, E. Secci, Visualization of redox-controlled protein fold in living cells. *Chem Biol* 2013, *20*. 747-52, DOI: S1074-5521(13)00210-X [pii]

10.1016/j.chembiol.2013.05.007.

11. (a) C. J. Stork, Y. V. Li, Intracellular zinc elevation measured with a "calcium-specific" indicator during ischemia and reperfusion in rat hippocampus: a question on calcium overload. *J Neurosci* 2006, *26*. 10430-7, DOI: 26/41/10430 [pii]

10.1523/JNEUROSCI.1588-06.2006; (b) Y. V. Medvedeva, B. Lin, C. W. Shuttleworth, J. H. Weiss, Intracellular Zn2+ accumulation contributes to synaptic failure, mitochondrial depolarization, and cell death in an acute slice oxygen-glucose deprivation model of ischemia. *J Neurosci* 2009, *29*. 1105-14, DOI: 29/4/1105 [pii]

10.1523/JNEUROSCI.4604-08.2009; (c) S. L. Sensi, P. Paoletti, J. Y. Koh, E. Aizenman, A. I. Bush, M. Hershfinkel, The neurophysiology and pathology of brain zinc. *J Neurosci* 2011, *31*. 16076-85, DOI: 31/45/16076 [pii]

10.1523/JNEUROSCI.3454-11.2011; (d) D. W. Choi, J. Y. Koh, Zinc and brain injury. *Annu Rev Neurosci* 1998, *21*. 347-75, DOI: 10.1146/annurev.neuro.21.1.347.

12. (a) W. Maret, Zinc and human disease. *Metal ions in life sciences* 2013, *13*. 389-414, DOI: 10.1007/978-94-007-7500-8_12; (b) S. S. Leal, H. M. Botelho, C. M. Gomes, Metal ions as modulators of protein conformation and misfolding in neurodegeneration. *Coordination Chemistry Reviews* 2012, *256*. 2253-2270, DOI: 10.1016/j.ccr.2012.04.004.

13. (a) A. P. Smith, N. M. Lee, Role of zinc in ALS. *Amyotroph Lateral Scler* 2007, *8*. 131-43, DOI: 779130675 [pii]

10.1080/17482960701249241; (b) B. K. Bitanihirwe, M. G. Cunningham, Zinc: the brain's dark horse. *Synapse* 2009, *63*. 1029-49, DOI: 10.1002/syn.20683.

14. C. Corona, A. Pensalfini, V. Frazzini, S. L. Sensi, New therapeutic targets in Alzheimer's disease: brain deregulation of calcium and zinc. *Cell Death Dis* 2011, *2*. e176, DOI: cddis201157 [pii]

10.1038/cddis.2011.57.

15. (a) S. Pfaender, A. M. Grabrucker, Characterization of biometal profiles in neurological disorders. *Metallomics* 2014, *6*. 960-77, DOI: 10.1039/c4mt00008k; (b) E. Tokuda, E. Okawa, S. Watanabe, S. I. Ono, S. L. Marklund, Dysregulation of intracellular copper homeostasis is common to transgenic mice expressing human mutant superoxide dismutase-1s regardless of their copper-binding abilities. *Neurobiol Dis* 2013. DOI: S0969-9961(13)00013-2 [pii] 10.1016/j.nbd.2013.01.001; (c) Q. X. Li, S. S. Mok, K. M. Laughton, C. A. McLean, I. Volitakis, R. A. Cherny, N. S. Cheung, A. R. White, C. L. Masters, Overexpression of Abeta is associated with acceleration of onset of motor impairment and superoxide dismutase 1 aggregation in an amyotrophic lateral sclerosis mouse model. *Aging Cell* 2006, *5*. 153-65, DOI: ACE200 [pii] 10.1111/j.1474-9726.2006.00200.x; (d) H. L. Lelie, A. Liba, M. W. Bourassa, M. Chattopadhyay, P. K. Chan, E. B. Gralla, L. M. Miller, D. R. Borchelt, J. S. Valentine, J. P. Whitelegge, Copper and zinc metallation status of copper-zinc superoxide dismutase from amyotrophic lateral sclerosis transgenic mice. *J Biol Chem* 2011, *286*. 2795-806, DOI: M110.186999 [pii] 10.1074/jbc.M110.186999.

16. J. Kim, T. Y. Kim, J. J. Hwang, J. Y. Lee, J. H. Shin, B. J. Gwag, J. Y. Koh, Accumulation of labile zinc in neurons and astrocytes in the spinal cords of G93A SOD-1 transgenic mice. *Neurobiol Dis* 2009, *34*. 221-9, DOI: S0969-9961(09)00006-0 [pii] 10.1016/j.nbd.2009.01.004.

17. A. Spalloni, N. Origlia, C. Sgobio, A. Trabalza, M. Nutini, N. Berretta, G. Bernardi, L. Domenici, M. Ammassari-Teule, P. Longone, Postsynaptic alteration of NR2A subunit and defective autophosphorylation of alphaCaMKII at threonine-286 contribute to abnormal plasticity and morphology of upper motor neurons in presymptomatic SOD1G93A mice, a murine model for amyotrophic lateral sclerosis. *Cereb Cortex* 2011, *21*. 796-805, DOI: bhq152 [pii] 10.1093/cercor/bhq152.

18. I. Bertini, M. Piccioli, M. S. Viezzoli, C. Y. Chiu, G. T. Mullenbach, A spectroscopic characterization of a monomeric analog of copper, zinc superoxide dismutase. *European biophysics journal : EBJ* 1994, *23*. 167-76.

19. J. S. Valentine, P. A. Doucette, S. Zittin Potter, Copper-zinc superoxide dismutase and amyotrophic lateral sclerosis. *Annu Rev Biochem* 2005, *74*. 563-93, DOI: 10.1146/annurev.biochem.72.121801.161647.

20. K. M. Beem, W. E. Rich, K. V. Rajagopalan, Total reconstitution of copper-zinc superoxide dismutase. *J Biol Chem* 1974, *249*. 7298-305.

21. V. H. Le, R. Buscaglia, J. B. Chaires, E. A. Lewis, Modeling complex equilibria in isothermal titration calorimetry experiments: thermodynamic parameters estimation for a three-binding-site model. *Anal Biochem* 2013, *434*. 233-41, DOI: S0003-2697(12)00623-9 [pii] 10.1016/j.ab.2012.11.030.

22. E. Luchinat, L. Barbieri, J. T. Rubino, T. Kozyreva, F. Cantini, L. Banci, In-cell NMR reveals potential precursor of toxic species from SOD1 fALS mutants. *Nature communications* 2014, *5*. 5502, DOI: 10.1038/ncomms6502.

23. A. L. Lamb, A. S. Torres, T. V. O'Halloran, A. C. Rosenzweig, Heterodimeric structure of superoxide dismutase in complex with its metallochaperone. *Nat Struct Biol* 2001, *8*. 751-5, DOI: 10.1038/nsb0901-751 nsb0901-751 [pii].

24. A. E. Cass, H. A. Hill, J. V. Bannister, W. H. Bannister, Zinc(II) binding to apo-(bovine erythrocyte superoxide dismutase). *Biochem J* 1979, *177*. 477-86.

25. (a) F. Arnesano, L. Banci, I. Bertini, M. Martinelli, Y. Furukawa, T. V. O'Halloran, The unusually stable quaternary structure of human Cu,Zn-superoxide dismutase 1 is controlled by both metal occupancy and disulfide status. *J Biol Chem* 2004, *279*. 47998-8003, DOI: 10.1074/jbc.M406021200 M406021200 [pii]; (b) L. Banci, I. Bertini, F. Cantini, N. D'Amelio, E. Gaggelli, Human SOD1 before harboring the catalytic metal: solution structure of copper-depleted, disulfide-reduced form. *J Biol Chem* 2006, *281*. 2333-7, DOI: M506497200 [pii] 10.1074/jbc.M506497200.

26. D. K. Wilkins, S. B. Grimshaw, V. Receveur, C. M. Dobson, J. A. Jones, L. J. Smith, Hydrodynamic radii of native and denatured proteins measured by pulse field gradient NMR techniques. *Biochemistry* 1999, *38*. 16424-31, DOI: bi991765q [pii].

27. (a) A. R. Ferre-D'Amare, S. K. Burley, Use of dynamic light scattering to assess crystallizability of macromolecules and macromolecular assemblies. *Structure* 1994, *2*. 357-9; (b) U. Nobbmann, M. Connah, B. Fish, P. Varley, C. Gee, S. Mulot, J. Chen, L. Zhou, Y. Lu, F. Shen, J. Yi, S. E. Harding, Dynamic light scattering as a relative tool for assessing the molecular integrity and stability of monoclonal antibodies. *Biotechnol Genet Eng Rev* 2007, *24*. 117-28.

28. L. Banci, I. Bertini, M. Boca, V. Calderone, F. Cantini, S. Girotto, M. Vieru, Structural and dynamic aspects related to oligomerization of apo SOD1 and its mutants. *Proc Natl Acad Sci U S A* 2009, *106*. 6980-5, DOI: 0809845106 [pii] 10.1073/pnas.0809845106.

29. S. V. Seetharaman, D. D. Winkler, A. B. Taylor, X. Cao, L. J. Whitson, P. A. Doucette, J. S. Valentine, V. Schirf, B. Demeler, M. C. Carroll, V. C. Culotta, P. J. Hart, Disrupted zinc-binding sites in structures of pathogenic SOD1 variants D124V and H80R. *Biochemistry* 2010, *49*. 5714-25, DOI: 10.1021/bi100314n.

30. W. Maret, Y. Li, Coordination dynamics of zinc in proteins. *Chemical reviews* 2009, *109*. 4682-707, DOI: 10.1021/cr800556u.

31. T. Miura, K. Suzuki, N. Kohata, H. Takeuchi, Metal binding modes of Alzheimer's amyloid beta-peptide in insoluble aggregates and soluble complexes. *Biochemistry* 2000, *39*. 7024-31, DOI: bi0002479 [pii].

32. L. S. Field, Y. Furukawa, T. V. O'Halloran, V. C. Culotta, Factors controlling the uptake of yeast copper/zinc superoxide dismutase into mitochondria. *J Biol Chem* 2003, *278*. 28052-9, DOI: 10.1074/jbc.M304296200 M304296200 [pii].

33. A. Nordlund, L. Leinartaite, K. Saraboji, C. Aisenbrey, G. Grobner, P. Zetterstrom, J. Danielsson, D. T. Logan, M. Oliveberg, Functional features cause misfolding of the ALS-provoking enzyme SOD1. *Proc Natl Acad Sci U S A* 2009, *106*. 9667-72, DOI: 0812046106 [pii] 10.1073/pnas.0812046106.

34. (a) B. F. Shaw, J. S. Valentine, How do ALS-associated mutations in superoxide dismutase 1 promote aggregation of the protein? *Trends Biochem Sci* 2007, *32*. 78-85, DOI: S0968-0004(06)00333-1 [pii] 10.1016/j.tibs.2006.12.005; (b) E. Sandelin, A. Nordlund, P. M. Andersen, S. S. Marklund, M. Oliveberg, Amyotrophic lateral sclerosis-associated copper/zinc superoxide dismutase

mutations preferentially reduce the repulsive charge of the proteins. *J Biol Chem* 2007, *282*. 21230-6, DOI: M700765200 [pii]
10.1074/jbc.M700765200.

35. Y. Shi, R. A. Mowery, B. F. Shaw, Effect of metal loading and subcellular pH on net charge of superoxide dismutase-1. *J Mol Biol* 2013, *425*. 4388-404, DOI: S0022-2836(13)00452-X [pii]
10.1016/j.jmb.2013.07.018.

36. (a) A. Hawe, M. Sutter, W. Jiskoot, Extrinsic fluorescent dyes as tools for protein characterization. *Pharm Res* 2008, *25*. 1487-99, DOI: 10.1007/s11095-007-9516-9; (b) H. LeVine, 3rd, Quantification of beta-sheet amyloid fibril structures with thioflavin T. *Methods Enzymol* 1999, *309*. 274-84, DOI: S0076-6879(99)09020-5 [pii]; (c) H. LeVine, 3rd, Thioflavine T interaction with synthetic Alzheimer's disease beta-amyloid peptides: detection of amyloid aggregation in solution. *Protein Sci* 1993, *2*. 404-10, DOI: 10.1002/pro.5560020312; (d) M. Biancalana, S. Koide, Molecular mechanism of Thioflavin-T binding to amyloid fibrils. *Biochim Biophys Acta* 2010, *1804*. 1405-12, DOI: S1570-9639(10)00099-3 [pii]
10.1016/j.bbapap.2010.04.001; (e) A. Jan, O. Gokce, R. Luthi-Carter, H. A. Lashuel, The ratio of monomeric to aggregated forms of Abeta40 and Abeta42 is an important determinant of amyloid-beta aggregation, fibrillogenesis, and toxicity. *J Biol Chem* 2008, *283*. 28176-89, DOI: M803159200 [pii]
10.1074/jbc.M803159200; (f) I. Maezawa, H. S. Hong, R. Liu, C. Y. Wu, R. H. Cheng, M. P. Kung, H. F. Kung, K. S. Lam, S. Oddo, F. M. Laferla, L. W. Jin, Congo red and thioflavin-T analogs detect Abeta oligomers. *J Neurochem* 2008, *104*. 457-68, DOI: JNC4972 [pii]
10.1111/j.1471-4159.2007.04972.x; (g) M. Necula, R. Kayed, S. Milton, C. G. Glabe, Small molecule inhibitors of aggregation indicate that amyloid beta oligomerization and fibrillization pathways are independent and distinct. *J Biol Chem* 2007, *282*. 10311-24, DOI: M608207200 [pii]
10.1074/jbc.M608207200.

37. L. Banci, I. Bertini, M. Boca, S. Girotto, M. Martinelli, J. S. Valentine, M. Vieru, SOD1 and amyotrophic lateral sclerosis: mutations and oligomerization. *PLoS One* 2008, *3*. e1677, DOI: 10.1371/journal.pone.0001677.

38. Y. Yoshimura, Y. Lin, H. Yagi, Y. H. Lee, H. Kitayama, K. Sakurai, M. So, H. Ogi, H. Naiki, Y. Goto, Distinguishing crystal-like amyloid fibrils and glass-like amorphous aggregates from their kinetics of formation. *Proc Natl Acad Sci U S A* 2012, *109*. 14446-51, DOI: 1208228109 [pii]
10.1073/pnas.1208228109.

39. S. S. Leal, I. Cardoso, J. S. Valentine, C. M. Gomes, Calcium Ions Promote Superoxide Dismutase 1 (SOD1) Aggregation into Non-fibrillar Amyloid: A LINK TO TOXIC EFFECTS OF CALCIUM OVERLOAD IN AMYOTROPHIC LATERAL SCLEROSIS (ALS)? *J Biol Chem* 2013, *288*. 25219-28, DOI: 10.1074/jbc.M113.470740.

40. P. B. Stathopulos, J. A. O. Rumfeldt, G. A. Scholz, R. A. Irani, H. E. Frey, R. A. Hallewell, J. R. Lepock, E. M. Meiering, Cu/Zn superoxide dismutase mutants associated with amyotrophic lateral sclerosis show enhanced formation of aggregates in vitro. *Proceedings of the National Academy of Sciences* 2003, *100*. 7021-7026, DOI: 10.1073/pnas.1237797100.

41. L. C. Serpell, J. Berriman, R. Jakes, M. Goedert, R. A. Crowther, Fiber diffraction of synthetic alpha-synuclein filaments shows amyloid-like cross-beta conformation. *Proc Natl Acad Sci U S A* 2000, *97*. 4897-902.

42. M. Sunde, L. C. Serpell, M. Bartlam, P. E. Fraser, M. B. Pepys, C. C. Blake, Common core structure of amyloid fibrils by synchrotron X-ray diffraction. *J Mol Biol* 1997, *273*. 729-39, DOI: S0022-2836(97)91348-6 [pii]
10.1006/jmbi.1997.1348.

43. Y. Furukawa, K. Kaneko, K. Yamanaka, N. Nukina, Mutation-dependent polymorphism of Cu,Zn-superoxide dismutase aggregates in the familial form of amyotrophic lateral sclerosis. *J Biol Chem* 2010, *285*. 22221-31, DOI: 10.1074/jbc.M110.113597.

44. (a) B. J. Turner, K. Talbot, Transgenics, toxicity and therapeutics in rodent models of mutant SOD1-mediated familial ALS. *Progress in neurobiology* 2008, *85*. 94-134, DOI: 10.1016/j.pneurobio.2008.01.001; (b) J. Wang, G. Xu, H. Li, V. Gonzales, D. Fromholt, C. Karch, N. G. Copeland, N. A. Jenkins, D. R. Borchelt, Somatodendritic accumulation of misfolded SOD1-L126Z in motor neurons mediates degeneration: αB-crystallin modulates aggregation. *Human Molecular Genetics* 2005, *14*. 2335-2347, DOI: 10.1093/hmg/ddi236; (c) T. Gidalevitz, T. Krupinski, S. Garcia, R. I. Morimoto, Destabilizing protein polymorphisms in the genetic background direct phenotypic expression of mutant SOD1 toxicity. *PLoS genetics* 2009, *5*. e1000399, DOI: 10.1371/journal.pgen.1000399.

45. R. W. Strange, S. V. Antonyuk, M. A. Hough, P. A. Doucette, J. S. Valentine, S. S. Hasnain, Variable metallation of human superoxide dismutase: atomic resolution crystal structures of Cu-Zn, Zn-Zn and as-isolated wild-type enzymes. *J Mol Biol* 2006, *356*. 1152-62.

46. (a) R. Bystrom, P. M. Andersen, G. Grobner, M. Oliveberg, SOD1 mutations targeting surface hydrogen bonds promote amyotrophic lateral sclerosis without reducing apo-state stability. *J Biol Chem* 2010, *285*. 19544-52, DOI: M109.086074 [pii]
10.1074/jbc.M109.086074; (b) J. A. Rodriguez, B. F. Shaw, A. Durazo, S. H. Sohn, P. A. Doucette, A. M. Nersissian, K. F. Faull, D. K. Eggers, A. Tiwari, L. J. Hayward, J. S. Valentine, Destabilization of apoprotein is insufficient to explain Cu,Zn-superoxide dismutase-linked ALS pathogenesis. *Proc Natl Acad Sci U S A* 2005, *102*. 10516-21, DOI: 0502515102 [pii]
10.1073/pnas.0502515102.

47. M. Prudencio, P. J. Hart, D. R. Borchelt, P. M. Andersen, Variation in aggregation propensities among ALS-associated variants of SOD1: correlation to human disease. *Hum Mol Genet* 2009, *18*. 3217-26.

48. I. M. Ahl, M. J. Lindberg, L. A. Tibell, Coexpression of yeast copper chaperone (yCCS) and CuZn-superoxide dismutases in Escherichia coli yields protein with high copper contents. *Protein Expr Purif* 2004, *37*. 311-9, DOI: 10.1016/j.pep.2004.06.006 S1046592804001913 [pii].

49. J. P. Crow, J. B. Sampson, Y. Zhuang, J. A. Thompson, J. S. Beckman, Decreased zinc affinity of amyotrophic lateral sclerosis-associated superoxide dismutase mutants leads to enhanced catalysis of tyrosine nitration by peroxynitrite. *J Neurochem* 1997, *69*. 1936-44.

50. (a) A. Biesemeier, U. Schraermeyer, O. Eibl, Chemical composition of melanosomes, lipofuscin and melanolipofuscin granules of human RPE tissues. *Exp Eye Res* 2011, *93*. 29-39, DOI: S0014-4835(11)00112-6 [pii]

10.1016/j.exer.2011.04.004; (b) A. Biesemeier, U. Schraermeyer, O. Eibl, Quantitative chemical analysis of ocular melanosomes in stained and non-stained tissues. *Micron* 2011, *42*. 461-70, DOI: S0968-4328(11)00005-9 [pii]
10.1016/j.micron.2011.01.004.
51. O. Eibl, S. Schultheiss, P. Blitgen-Heinecke, U. Schraermeyer, Quantitative chemical analysis of ocular melanosomes in the TEM. *Micron* 2006, *37*. 262-76, DOI: S0968-4328(05)00130-7 [pii]
10.1016/j.micron.2005.08.006.